Research Article

iMedPub Journals
http://www.imedpub.com

Nano Research & Applications
ISSN 2471-9838

2016
Vol. 2 No. 1:14

Phase, Composition and Morphology Study and Analysis of Os-Pd/HfC Nanocomposites

A Heidari and C Brown

Faculty of Chemistry, California South University, 14731 Comet St. Irvine, CA 92604, USA

Corresponding author: A Heidari

scholar.researcher.scientist@gmail.com

Faculty of Chemistry, California South University, 14731 Comet St. Irvine, CA 92604, USA.

Tel: +1-775-410-4974

Citation: Heidari A, Brown C. Phase, Composition and Morphology Study and Analysis of Os-Pd/HfC Nanocomposites. Nano Res Appl. 2016, 2:1.

Abstract

In the current research, nanocomposites of Os-Pd/HfC were synthesized using thermal decomposition of solid state from Schiff base complexes of Osmium(IV) with formula of trans–bis(benzenethiolato) [N,N'–ethylenebis (salicylideneaminoato)] osmium(IV) and cis–bis(benzenethiolato) [N,N'–ethylene bis(salicylideneaminoato)] osmium(IV). The synthesized nanocomposites and the synthesized Schiff base complexes were identified using ATR–FTIR, XRD, SEM, TEM and EDX techniques. Also, electrical sedimentation of Os-Pd/HfC nanocomposites was studied. The effects of parameters such as amount of cathode rotation, applying ultrasonic waves and magnetic stirring were investigated. Further, the effect of Hafnium (IV) Carbide grading on the electrochemical sedimentation of the nanocomposites was studied. Hafnium (IV) Carbide with high level of purity was produced and precipitated using combustion synthesis method. The composition and morphology of composite were evaluated by ATR–FTIR, XRD, SEM, TEM and EDX. Moreover, the size of grains was calculated based on Scherrer equation and using X`Pert High Score Plus software. Furthermore, the production process of 2wt% Os-Pd/HfC and 4wt% Os-Pd/HfC nanocomposites powders by thermochemical method was investigated. The produced phases in various steps of heat treatment were identified by DTA–TGA, ATR–FTIR, XRD, SEM, TEM and EDX analyses.

Keywords: Os-Pd/HfC nanocomposites; Composition; Morphology; Phase analysis

Abbreviations: SEM: Scanning Electron Microscope; XRD: X–Ray Diffraction; ATR-FTIR: Attenuated Total Reflectance Fourier Transform Infrared Spectroscopy; TEM: Transmission Electron Microscope; DTA–TGA: Differential Thermal Analysis-Thermal Gravim Analysis; EDX: Energy–Dispersive X–Ray Spectroscopy

Received: February 05, 2016; **Accepted:** February 24, 2016; **Published:** February 29, 2016

Introduction

Recently, many research groups have been interested in nanocomposites of metal Oxides due to their various and numerous applications [1-8]. Nanocomposites of Os-Pd/HfC have a wide range of applicability including magnetic and catalytic materials, super capacitors and Lithium batteries [9-19]. Various methods have been used to synthesize nanocomposites of Os-Pd/HfC [20-25] among those, Thermal Decomposition Method (TDM) (solo–thermal and solid state) is the most applicable method due to low costs of in used apparatuses as well as good control on appropriate conditions for producing nanocomposites with desirable size and morphology [26-30]. In the current research, Schiff base complexes of Osmium(IV) with formula of trans–bis(benzenethiolato) [N,N'–ethylene bis(salicylideneaminoato)] osmium(IV) and cis–bis(benzenethiolato) [N,N'ethylenebis (salicylideneaminoato)] osmium(IV) were synthesized, at first, and then, nanocomposites of Os-Pd/HfC were synthesized in an oven at 475°C during 4 hours **(Figures 1 and 2).**

Hafnium (IV) Carbide is a hard compound with high melting temperature and electrical conductivity. The Osmium based composites, especially those contain hard ceramic particles; have been considered as covers resistant to abrasion in high temperatures. Osmium composites containing HfC particles are developed as hard cover for steel rollers and covers of injective molds [31-39].

The electrical precipitation of Osmium using Osmium bathes

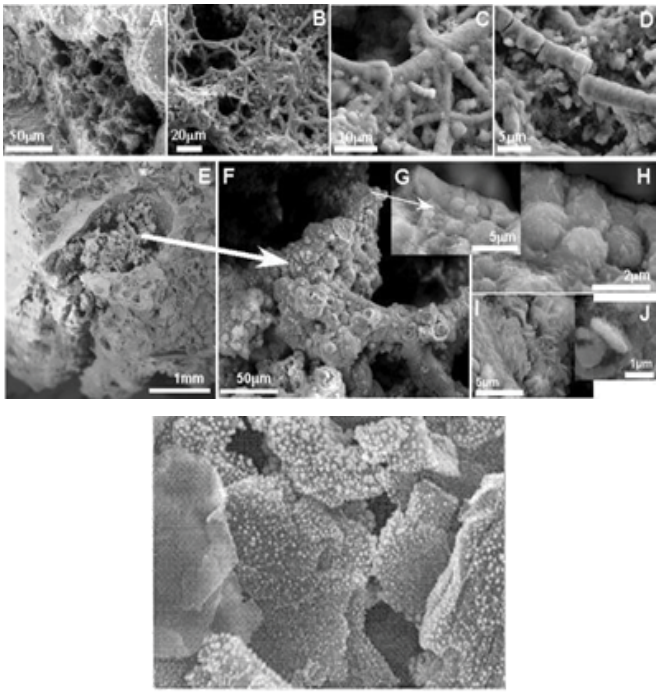

Figure 1 SEM images of Os-Pd/HfC nanocomposites in different scales with (A) 70000x zoom, (B) 70000x zoom, (C) 100000x zoom, (D) 100000x zoom, (E) 120000x zoom, (F) 140000x zoom, (G) 160000x zoom, (H) 170000x zoom, (I) 180000x zoom and (J) 190000x zoom (upper illustration) and TEM image of Os-Pd/HfC nanocomposites with 130000x zoom (lower illustration).

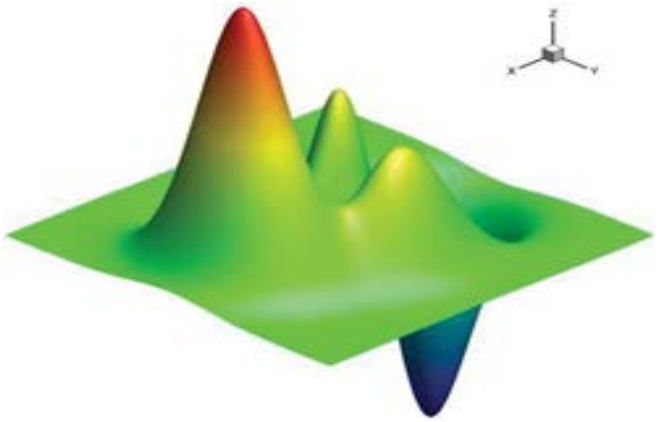

Figure 2 Simulated potential energy surfaces for the formation of Os-Pd/HfC nanocomposites wherein the x and y axes show intrinsic reaction coordinates (IRC) and the z–axis shows energy.

performs based on Phosphoraniminato or Nitrido and is of some advantages such as: (1) Easy storing of electrolyte; (2) Availability of Osmium(IV) Phosphoraniminato and Osmium(VI) Nitrido with high purity and reasonable cost; and (3) Creating layers with low brittleness and internal tension. Although Palladium Flvbvrat bath was used by Bapu to synthesize Os-Pd/HfC composite, the produced composite was not in nano size. Most of Os-Pd/HfC electrical precipitation composites have patent and their details are not available [40-47].

There are various methods for synthesizing nanocomposites; the most important of those are including: mechanical alloying [48,49] combustion synthesis [50,51] and electrochemical precipitation [52-57]. It is difficult to synthesize some types of composites by usual methods due to very low wetting of hard phase by melt of background phase. The electrochemical synthesize of this composite can solve this problem to some extent. At the other side, covering industrial pieces by composite materials is generally implemented by thermal spraying and PVD; severe oxidation will be possible during those methods. While the electrochemical methods are of simple system and does not need to complex apparatuses, those have not the oxidation problem [53-59].

This method is environmentally friendly and it is controllable. However, the mechanical alloying has not desirable quality because of high residual stress. As a result, the objective of the current study is producing Os-Pd/HfC composites using simple electrochemical method which avoids these deficiencies.

Productions of ceramics, composites and refractory materials using combustion synthesis method have been widely studied during last two decades. In this method, various mixed and compacted powders ignite in the air or neutral atmosphere and the combustion face produce by performing an exothermic chemical reaction. Then, products constitute by passing this face through reagents [60-65].

Osmium can be strengthened by integrating with fine ceramic particles; however, it causes a little decrease in electrical conductivity of Osmium [66-69]. Metal matrix composites of Osmium reinforced with Palladium–Hafnium (IV) Carbide integrate high electrical conductivity of Osmium with high chemical–thermal ability and high strength of Palladium–Hafnium (IV) Carbide phase; therefore, Os-Pd/HfC composites are of ability to represent high strength and electrical conductivity [70-73]. The structure of Osmium matrix nanocomposites need to a uniform distribution of nano sized reinforcing particles to show high strength and high abrasion resistance [74,75]. As a result, production method of these nanocomposites to achieve a uniform distribution and nano sized particles is of critical importance [76,77].

In situ technique is being used to produce this nanocomposite in which reinforced particles are being created through chemical reactions during production process of nanocomposites and it leads to creating very fine sized particles with uniform distribution [78,79].

There are various methods for producing Osmium matrix nanocomposites such as internal oxidation, mechanical alloying and thermochemical method. Non–uniform distribution of Oxide particles negatively affects the electrical and mechanical properties of this nanocomposite [80,81]. The previously performed studies [82,83] have been shown that more uniform distribution of particles, along with a nano sized structure, can be obtained using thermochemical method which improves electrical and mechanical properties of this nanocomposite [84,85].

Furthermore, it should be noted that in the current research,

Os-Pd/HfC nanocomposites powder containing 2 and 4 weight percent of Palladium–Hafnium (IV) Carbide were produced by thermochemical method and the produced phases in various steps of heat treatment to synthesize the final nanocomposites powder were studied.

Materials, Research Method and Experimental Techniques

All chemical materials (solvents, amines, aldehydes and so on) used in the current research were bought from Sigma–Aldrich company and were utilized without any purification. The vibration spectra of ligands, associated complexes and resulted nanocomposites, in the range of 400 cm^{-1} and 4000 cm^{-1}, are derived by Attenuated Total Reflectance Fourier Transform Infrared Spectroscopy (ATR–FTIR) Bruker. The elemental analysis is performed by 2400 CHN Elemental Analyzer by Perkin Elmer apparatus. The X-Ray Diffraction (XRD) spectra of compounds are achieved by PAN alytical-X 'Pert Pro MPD with Cr *Kα* rays in the angle range of 2θ = 5°–80°. Scanning Electron Microscope (SEM) images are captured by scanning electron microscope apparatus of Cam Scan MV2300. The Transmission Electron Microscope (TEM) apparatus used in this study was Cs–corrected Dedicated TEM HD–2700. The model of Differential Thermal Analysis-Thermal Gravim Analysis (DTA–TGA) apparatus where used was Perkin STA 8000/ST–740 Series and the Energy-Dispersive X–Ray Spectroscopy (EDX) apparatus was RONTEC–QUANTAX/QX2.

To synthesize nanocomposites of Os-Pd/HfC, some amount of complexes trans-bis(benzenethiolato) [N,N'–ethylene bis (salicylideneaminoato)] osmium(IV) and cis-bis (benzenethiolato) [N,N'–ethylenebis(salicylide neaminoato)]osmium(IV) were uniformly powdered in a crucible, at first, and then, the obtained powder was set into an electric oven under 475°C. After about 4 hours, the resulted gray powder was washed by methanol and the final product was filtered and dried in the air. For identifying the final product, ATR– FTIR was used. Since the obtained precipitation has not residual stress, the grain size can be easily calculated by Scherrer equation as [86,87]:

$$D = 0.9\lambda / \beta.\cos\theta$$

where λ is wavelength in Angstrom, θ is angle of diffraction and β is peak width at the half height of the maximum intensity in terms of radians. In the current research, grain sizes are calculated by X`Pert HighScore Plus software based on Scherrer equation.

The production process of Os– Pd/HfC nanocomposites powder consists of the following steps:

1. Preparing aqueous solution of Osmium(IV) Phosphoraniminato and Osmium(VI) Nitrido in proportion with final composition of the product (Os–Pd/HfC nanocomposites containing 2 and 4 weight percent of Palladium– Hafnium (IV) Carbide).
2. Heating the aqueous solution and creating the elementary powder.
3. Thermal desalination process of the produced powders in the air at 500°C for 4 hours.
4. Heat treatment to create Palladium– Hafnium (IV) Carbide at various temperatures of 650, 750, 850, 950, 1050, 1150, 1250 and 1350°C for two hours in the air.
5. Heat treatment of Osmium(IV) Phosphoraniminato and Osmium(VI) Nitrido reduction in the Hydrogen atmosphere at temperatures of 450, 550, 650, 750, 850, 950 and 1050°C for two hours to produce nanocomposites powder.

After thermal desalination process, powders were analyzed by ATR–FTIR, DTA–TGA, XRD, SEM, TEM and EDX. To better identification of phases after heat treatment at 1250°C, 15% Nitric acid solution was added to solve the presented Osmium(IV) Phosphoraniminato and Osmium(VI) Nitrido and to identify other compositions.

Results and Discussion

In the current research, nanocomposites of Os-Pd/HfC were synthesized using thermal decomposition of solid state from Schiff base complexes of Osmium(IV) with formula of trans–bis (benzenethiolato) [N,N'–ethylenebis (salicylideneaminoato)] osmium(IV) and cis–bis (benzenethiolato) [N,N'–ethylenebis (salicylideneaminoato)] osmium(IV) at 475°C during 4 hours. The synthesized nanocomposites and the synthesized Schiff base complexes were identified using ATR–FTIR, XRD, SEM, TEM and EDX techniques. The obtained results from these techniques were shown that the synthesized nanocomposites from Schiff base complexes have a plain structure while nanocomposites of Os-Pd/HfC synthesized from the complexes have cubic structure and their sizes are between 50 and 200 nanometers. Also, electrical sedimentation of Os-Pd/HfC nanocomposites were studied. The effects of parameters such as amount of cathode rotation, applying ultrasonic waves and magnetic stirring were investigated. Further, the effect of Hafnium (IV) Carbide grading on the electrochemical sedimentation of the nanocomposites was studied. Hafnium (IV) Carbide with high level of purity was produced and precipitated using combustion synthesis method. The composition and morphology of composite were evaluated by ATR–FTIR, XRD, SEM, TEM and EDX techniques. Moreover, the size of grains was calculated based on Scherrer equation and using X`Pert HighScore Plus software. It was observed that the best result is obtained from suspension containing the produced Hafnium (IV) Carbides by combustion synthesis and magnetic stirring method. Furthermore, the production processes of 2wt% Os-Pd/HfC and 4wt% Os-Pd/HfC nanocomposites powders by thermochemical method were investigated. The produced phases in various steps of heat treatment were identified by DTA–TGA, ATR–FTIR, XRD, SEM, TEM and EDX analyses. The nanocomposites powders were produced through the following steps: preparing aqueous solution of Osmium(IV) Phosphoraniminato and Osmium(VI) Nitrido to achieve final compound; heating the aqueous solution and creating the elementary powder; thermal desalination process; heat treatment to create Palladium–Hafnium(IV) Carbide at various temperatures and; reducing Osmium(IV) Phosphoraniminato and Osmium(VI) Nitrido to Osmium in various temperatures in Hydrogen atmosphere. Optimum temperatures for creating Palladium–Hafnium(IV) Carbide and reducing powders were obtained at 830 and 860°C, respectively. Size of the produced Palladium–Hafnium (IV) Carbide particles by thermochemical method was about 30–60 nanometers. The experimental results obtained from elemental analysis of associated complexes are presented in **Table 1.** Good agreement between theoretical and experimental results confirms the purity of synthesized compounds. It should be noted

that the elemental analysis is performed by 2400 CHN Elemental Analyzer by Perkin Elmer apparatus.

In vibration spectra of synthesized complexes, the related peak to vibrations of various groups can be seen that their most important one is the peak related to vibration of imine group (C=N) which is emerged in the range of 1610 and 1620 cm^{-1} (depend on the type of complex). The lack of the peak related to aldehyde and amine groups in these complexes demonstrate the lack of Schiff base ligand in these complexes. However, a peak related to vibration of piperidine in 3553 cm^{-1} can be observed in trans–bis (benzenethiolato) [N,N'-ethylenebis (salicylideneaminoato)] osmium(IV) complex in addition to imine peak. In the complexes synthesized in the current study, the peak related to vibration of aliphatic and aromatic Hydrogens is emerged in 3250 cm^{-1} and the peak related to vibrations of C=C ring can be observed in the range of 1350–1650 cm^{-1}. However, in the vibration spectra of the synthesized nanocomposites **(Figure 3)**, the only observable vibration peak is for Os–O group where is in the range of 569 to 663 cm^{-1}. The presence of these two peaks in the vibration spectra is a proof for constituting of the synthesized nanocomposites of Os-Pd/HfC **(Figure 3)**.

The XRD spectra of the synthesized complexes are shown in **Figure 4.** Comparison of the obtained XRD patterns for nanocomposites with the previously published results in this field confirms the presence of nanocomposites of Os– Pd/HfC **(Figure 4)**.

The obtained images from SEM of the complexes and the synthesized nanocomposites are shown in **Figure 5**. As can be seen, the nanocomposites obtained from the complexes (images a and b**, Figure 5)** are of approximately plain structure and the nanocomposites of Os– Pd/HfC resulted from the complexes (image c, **Figure 5)** have a cubic structure. The average size of the synthesized nanocomposites for complexes is in the range of 100–200 nanometers and for nanocomposites of Os– Pd/HfC is in the range of 50–100 nanometers **(Figures 5)**.

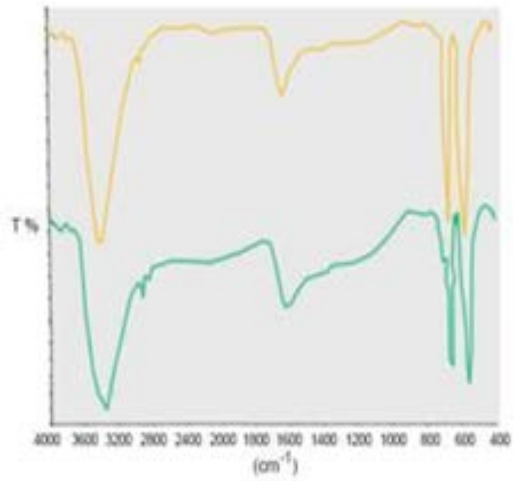

Figure 3 Vibration spectra of nanocomposites synthesized from trans-bis(benzenethiolato) [N,N'– ethylen ebis(salicylideneaminoato)]osmium (IV) (upper) and cis-bis(benzenethiolato)[N,N'ethylenebis (salicylideneaminoato)]osmium (IV) (lower) complexes.

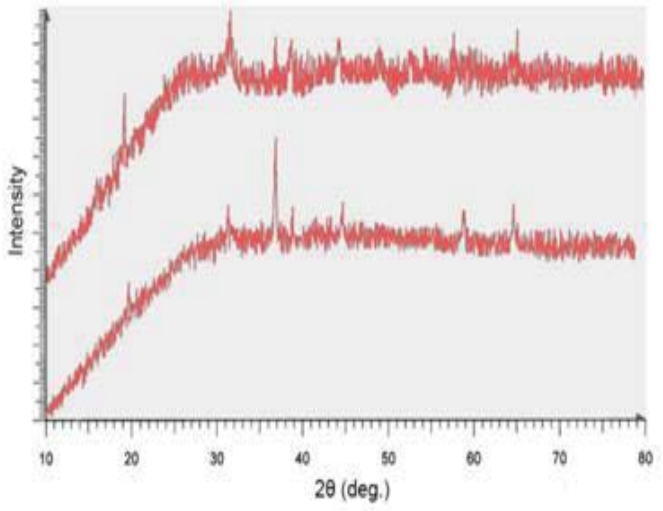

Figure 4 XRD spectra of nanocomposites synthesized from trans–bis(benzenethiolato)[N,N'– ethylenebis(salicylideneamin oato)]osmium (IV) (lower) and cis–bis(benzenethiolato) [N,N'– ethylenebis(salicylideneaminoato)]osmium (IV) (upper) complexes.

Figure (6) shows the pattern of the XRD results of the produced Hafnium (IV) Carbide by combustion synthesis. It can be concluded from this figure that the produced Hafnium (IV) Carbide by combustion synthesis is of high purity **(Figure 6)**.

The diffraction pattern of the produced precipitation is shown in **Figure 7**. The peaks related to Palladium and Hafnium (IV) Carbide are clearly shown in this figure. The high intensity of Pd peak is a sign of background phase and short peak of HfC indicates second (supportive) phase **(Figure 7**).

The results of SEM on precipitation are shown in **Figure 8** in which two produced phase regions (bright and dark regions) are clearly shown. Linear analysis of each phase shows that the bright region is Hafnium (IV) Carbide and the dark one is Palladium. It confirms the high stability of Hafnium (IV) Carbide phase **(Figure 8)**.

The hardness of the produced precipitation was 275 Vickers. The micro–hardness results obtained from various locations show 275–295 Vickers. The hardness can be uniformly seen through the precipitation which indicates uniform distribution of Hafnium (IV) Carbide in background and creating nanostructure. The governing mechanism on composite production is that as

Table 1 Experimental results of elemental analysis of synthesized complexes.

Complex	%C(Exp.)	%C(The.)	%H(Exp.)	%H(The.)	%N(Exp.)	%N(The.)
trans–bis(benzenethiolato)[N,N'–ethylenebis(salicylideneaminoato)]osmium(IV)	64.89	64.98	5.73	5.49	9.64	9.47
cis–bis(benzenethiolato)[N,N'–ethylenebis(salicylideneaminoato)]osmium(IV)	63.84	63.90	6.99	7.07	9.46	9.64

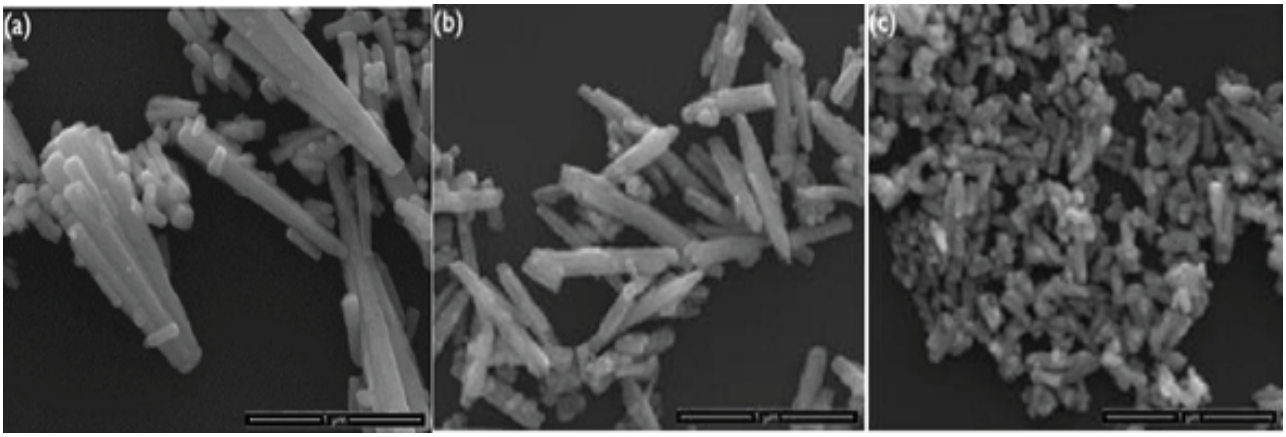

Figure 5 SEM images of (a) trans–bis(benzenethiolato)[N,N'–ethylenebis(salicylideneaminoato)]osmium(IV) with 120000x zoom, (b) cis–bis(benzenethiolato)[N,N'–ethylenebis(salicylideneaminoato)]osmium(IV) with 90000x zoom and (c) the resulted nanocomposites of Os– Pd/HfC with 60000x zoom.

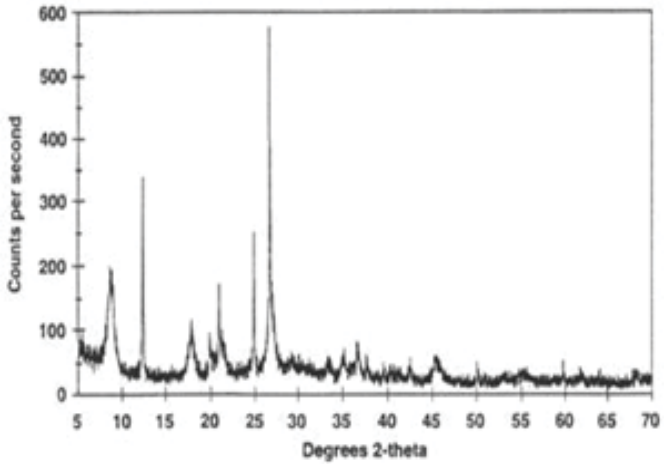

Figure 6 XRD pattern of the produced Hafnium (IV) Carbide by combustion synthesis.

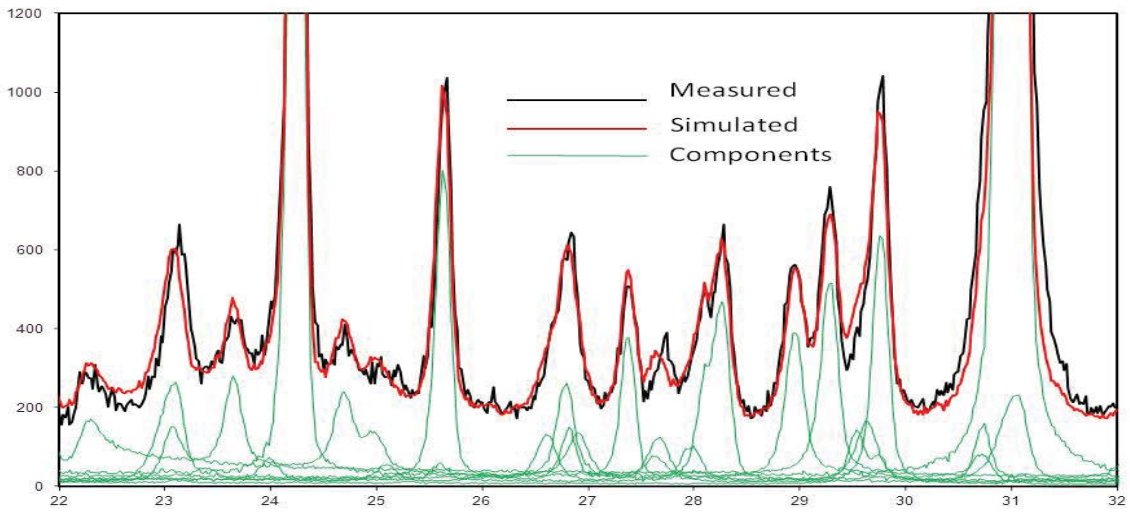

Figure 7 XRD pattern of the produced precipitation.

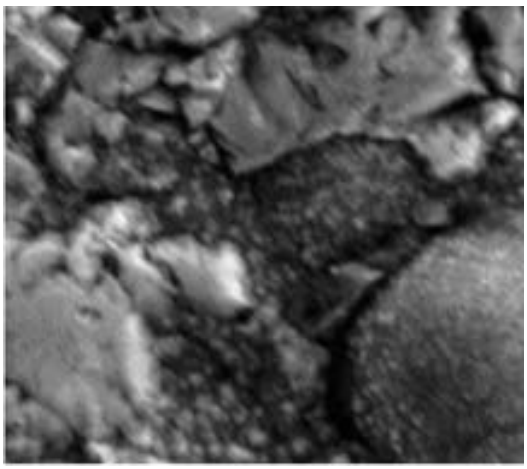

Figure 8 SEM image of the produced composite with 35000x zoom.

Palladium ions are reduced, Hafnium (IV) Carbide particles are placed between Palladium phase, at the same time, without any oxidation or reduction.

Based on the performed investigations, during electrical precipitation, Hydrogen and Oxygen absorbing led to producing complexes such as PdH^+ and $PdOH^+$. These compounds place on growth sites and prevent the growing of Palladium. Hence, a Palladium background with nanostructure will be produced.

After performing thermal desalination process (removing moisture and volatile compositions including Nitrates), XRD analysis was performed on the powders. Figure (9) shows the XRD pattern of powders with 4 weight percent of Palladium– Hafnium (IV) Carbide after thermal desalination process **(Figure 9).**

Regarding **Figure 9**, it can be seen that there are only peaks related to Osmium(IV) Phosphoraniminato and Osmium(VI) Nitrido phases in this figure. In this step, the peaks related to Palladium–Hafnium (IV) Carbide phase were not seen. Therefore, the next heat treatment was performed in the air at higher temperatures to synthesize stable Palladium– Hafnium (IV) Carbide phase. As the temperature in which Palladium– Hafnium (IV) Carbide phase is creating, the next heat treatments were performed on powders in the air at temperatures of 650, 750, 850, 950, 1050, 1150, 1250 and 1350°C for two hours **(Figure 9)**.

Figure 10 shows the experimental XRD related to various temperatures of heat treatment in the air to create Palladium–Hafnium (IV) Carbide phase. It can be seen that Palladium–Hafnium (IV) Carbide phase was emerged at 650°C and was completed at 860°C, so it can be said that temperatures higher than 650°C can overcome the activation energy for production process during heat treatment in the air. Regarding the fact that Palladium– Hafnium (IV) Carbide phase creation is completed at 860°C, it can be said that the optimum temperature for creation of Palladium– Hafnium (IV) Carbide phase is 860°C **(Figures 10)**.

Figure 11 shows the TEM images of Oxide powder after heat treatment for producing Palladium– Hafnium(IV) Carbide at 860°C. The black phase is related to Osmium(IV) Phosphoraniminato and Osmium(VI) Nitrido and fine spherical particles show Palladium - Hafnium(IV) Carbide phase. The size of Palladium– Hafnium (IV) Carbide particles obtained from TEM images is about 30–60 nanometers **(Figure 11)**.

After thermal desalination process, DTA–TGA analyses were performed on powders containing 2 and 4 weight percent of Palladium– Hafnium (IV) Carbide. **Figure 12** shows the DTA–TGA curves of these two powders **(Figure 12).**

Considering these figures, it can be seen that the DTA–TGA curves of powders containing 2 and 4 weight percent of Palladium– Hafnium (IV) Carbide are similar to each other. It was reported in the previously performed investigations that creation of Palladium - Hafnium (IV) Carbide phase cannot be seen on the DTA curve as a sharp and identified peak but the results obtained from XRD analysis was shown that creation of Palladium– Hafnium (IV) Carbide phase is started at 650°C. On the TGA curve, also, there is not a considerable weight change up to 850°C. However, about 15 percent decrease in weight can be observed at 850°C on both TGA curves and on corresponding DTA curves also an endothermic peak is being observed. Further, at about 1000°C, about 4 percent increase in weight is observed

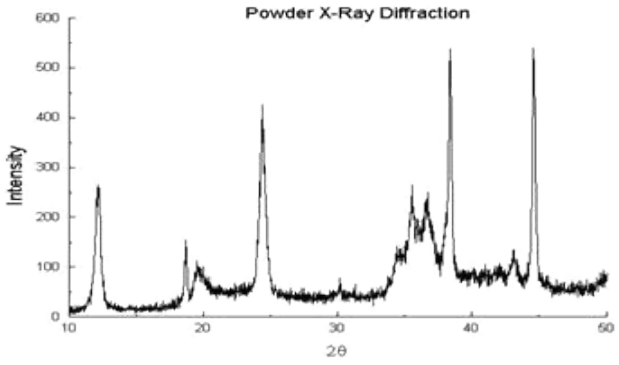

Figure 9 XRD pattern of powders containing 4 weight percent of Palladium–Hafnium (IV) Carbide and heat treated at 500°C for two hours.

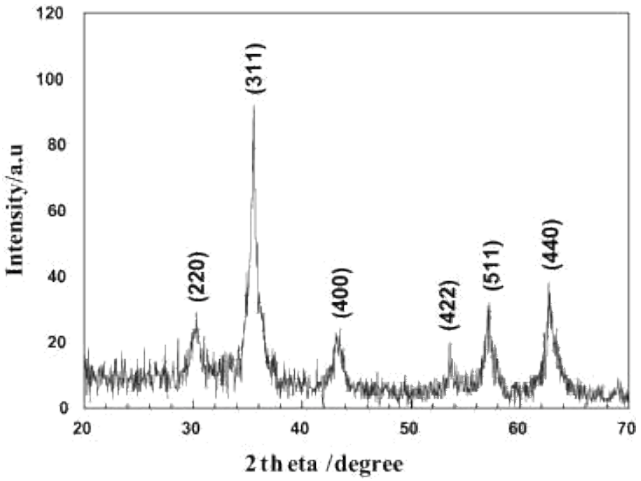

Figure 10 Experimental XRD pattern of powders containing 4 weight percent of Palladium– Hafnium (IV) Carbide and heat treated at (a) 650, (b) 750 and (c) 860°C for two hours.

on both TGA curves which are corresponding to an endothermic peak at temperature about 1000°C on both DTA curves.

To determine the produced phases in these two temperatures, powders were heat treated at two temperatures of 850 and 1000°C in the air for two hours and XRD analyses were performed on the obtained powders.

Figure 13 shows the XRD patterns of powders at 850 and 1000 degrees Celsius. Considering **Figure 13a**, it can be observed that in addition to the peaks related to Osmium(IV) Phosphoraniminato, Osmium(VI) Nitrido and Palladium - Hafnium(IV) Carbide phases, the peaks related to the third phase of Os– Pd/HfC also are presented. Therefore, it can be said that the endothermic peak at 850°C on the DTA curve indicates that Os– Pd/HfC is created **(Figure 13)**.

Figure 13b shows the XRD pattern of powders resulted from solving in Nitric acid solution. Considering **Figure 13b,** it can be observed that in addition to the peaks related to Palladium–Hafnium (IV) Carbide phase and Os– Pd/HfC, the peaks related to Osmium(IV) Phosphoraniminato and Osmium(VI) Nitrido also are presented at 1000°C. Therefore, considering the XRD results of heat treated powders at 850 and 1000°C, it can be said that two endothermic peaks on DTA curves of powders are related to creating trans–bis(benzenethiolato)[N,N'–ethylenebis(salicylideneaminoato)]osmium(IV) and cis–bis(benzenethiolato)[N,N'–ethylenebis(salicylideneaminoato)]osmium(IV) phases. It was reported in the previous studies [1–23,30] that after creation of Osmium(IV) Phosphoraniminato and Osmium(VI) Nitrido and Palladium– Hafnium (IV) Carbide due to mutual penetration of trans-bis(benzenethiolato)[N,N'-ethylenebis(salicylideneaminoato)]osmium(IV) and cis–bis(benzenethiolato)[N,N'-ethylenebis(salicylideneaminoato)]osmium(IV), Palladium– Hafnium (IV) Carbide phase is converted to Os–Pd/HfC phase **Figure (13)**.

The performed experiments were shown that the necessary temperature to reduce Osmium(IV) Phosphoraniminato and Osmium(VI) Nitrido to pure and elemental Osmium is 830°C and that in temperatures lower than 830°C, complete reduction of Osmium(IV) Phosphoraniminato and Osmium (VI) Nitrido to Osmium are not possible.

Figure 14 shows the experimental XRD patterns of heat treated powders in Hydrogen atmosphere at 830°C for two hours. Considering **Figure 14,** it can be observed that in this temperature, only peaks of Osmium phase are presented and Osmium(IV) Phosphoraniminato and Osmium(VI) Nitrido are completely reduced to Osmium. It is worthwhile to note that at reduction temperature of 830°C, the peaks related to Palladium– Hafnium (IV) Carbide phase are not presented. In fact, it is possible that uniform distribution of Palladium– Hafnium (IV) Carbide particles in the matrix of Osmium, nano sized Palladium - Hafnium(IV) Carbide particles and low percentage of those in the matrix of Osmium lead to lack of presence of Palladium– Hafnium(IV) Carbide peaks after the reduced treatment **(Figure 14)**.

Figure 15 shows the SEM image of powders containing 4 weights percent of Palladium - Hafnium (IV) Carbide after reduction treatment. Angular particles are Palladium– Hafnium (IV) Carbide phase and agglomerated spherical particles are Osmium phase **(Figure 15)**.

Figure 16 shows the curve related to EDX analysis of 4wt% Os-Pd/HfC powders after reduction treatment. An analysis was performed on these powders and the results were shown that this sample contains 4.84% Palladium– Hafnium (IV) Carbide and

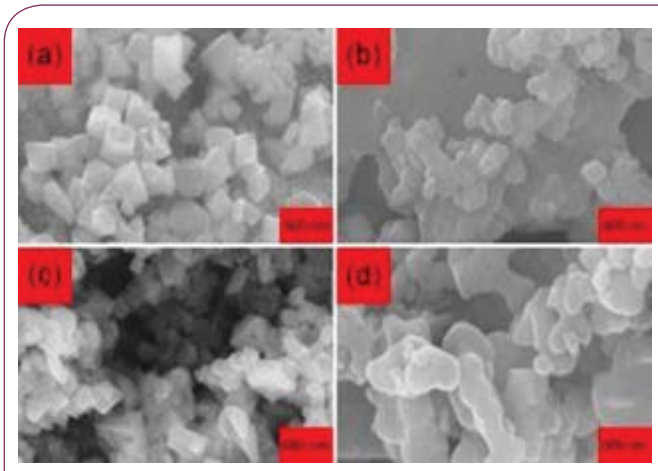

Figure 11 TEM images of powders containing 4 weight percent of Palladium– Hafnium (IV) Carbide and heat treated at (a) 800, (b) 830, (c) 860 and (d) 890°C for two hours with 100000x zoom.

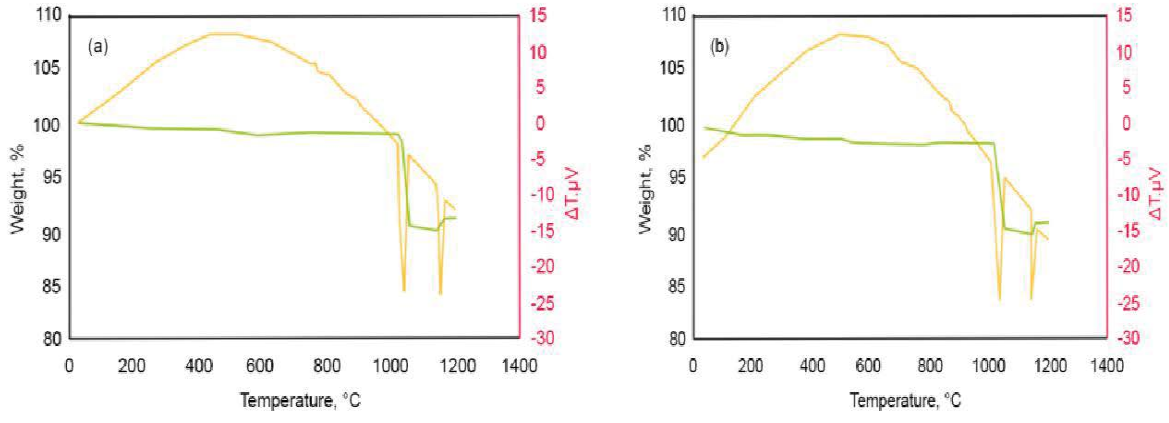

Figure 12 DTA–TGA curves of (a) 2wt% Os– Pd/HfC and (b) 4wt% Os– Pd/HfC produced by electrochemical method.

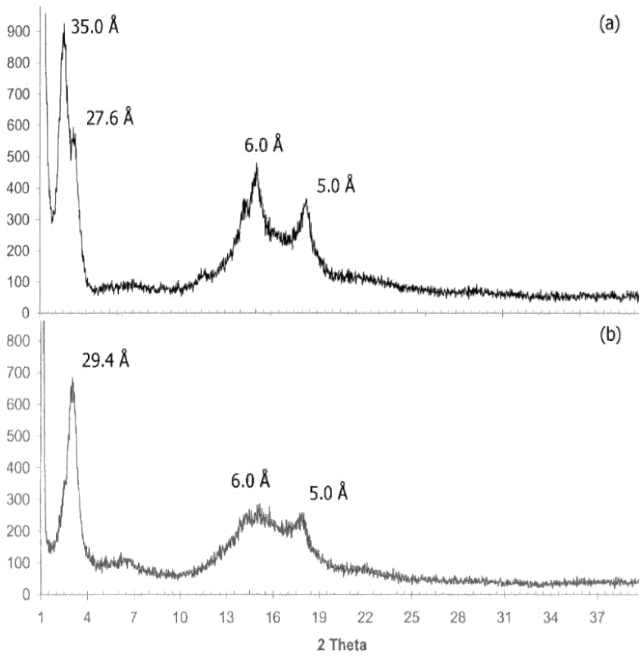

Figure 13 XRD pattern of powders containing 4 weight percent of Palladium– Hafnium (IV) Carbide and heat treated at (a) 850 and (b) 1000°C for two hours.

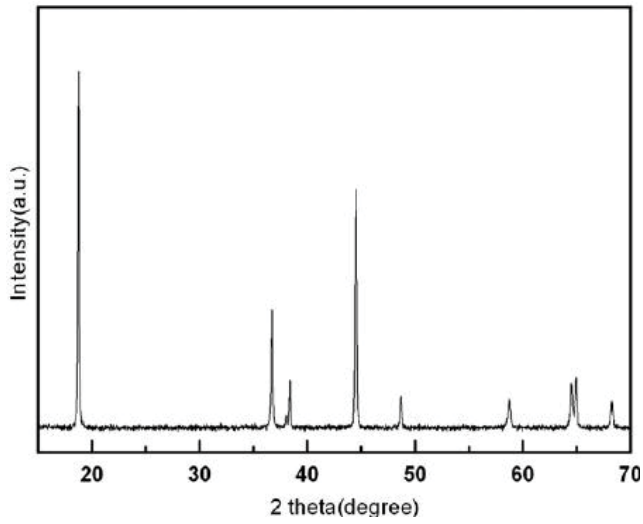

Figure 14 Experimental XRD pattern of powders containing 4 weights percent of Palladium– Hafnium (IV) Carbide and reduced in Hydrogen atmosphere at 830°C for two hours.

remaining of powders is Osmium **(Figure 16)**.

Figures 17 and 18 show simulated potential energy surfaces for the formation of Schiff base complexes of Osmium(IV) with formula of trans–bis(benzenethiolato)[N,N'–ethylenebis(salicylideneaminoato)]osmium(IV) and cis–bis (benzenethiolato) [N,N'–ethylenebis(salicylideneaminoato)] osmium(IV) at 475°C during 4 hours, respectively **(Figures 17 and 18)**.

Also, **Figures 19 and 20** illustrate simulated potential energy surfaces for the formation of Hafnium (IV) Carbide and Palladium– Hafnium (IV) Carbide, respectively **(Figures 19 and 20)**. Furthermore, **Figure 21** shows general outline of energy level graph of Os– Pd/HfC nanocomposites **(Figure 21)**.

Conclusion

By heating the Schiff base trans–bis(benzenethiolato)[N,N'–

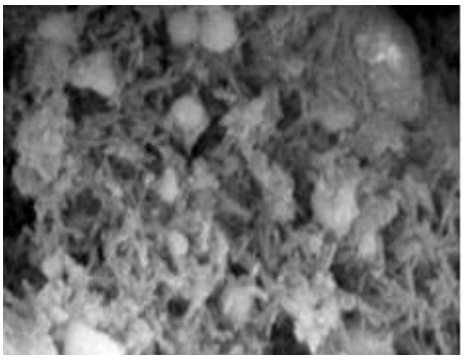

Figure 15 SEM image of 4wt% Os– Pd/HfC nanocomposites powders after reduction treatment with 110000x zoom.

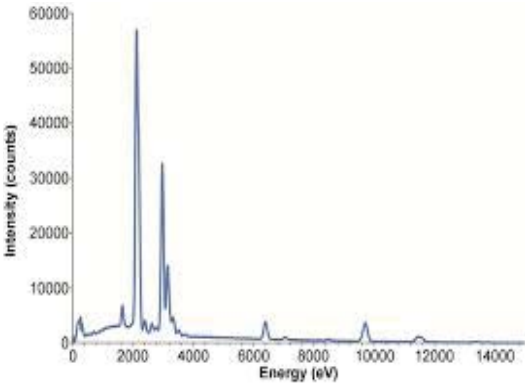

Figure 16 EDX analysis curve of 4wt% Os– Pd/HfC nanocomposites powders after reduction treatment.

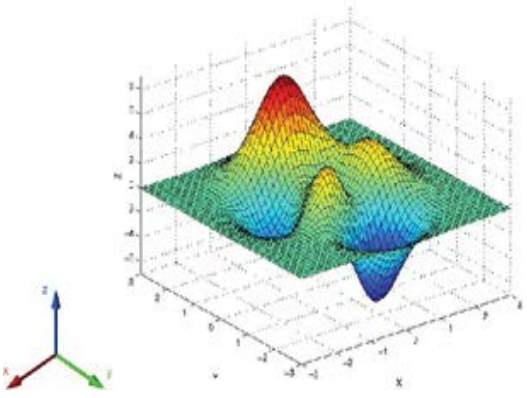

Figure 17 Simulated potential energy surfaces for the formation of Schiff base complex trans– bis(benzenethiolato)[N,N'–ethylenebis(salicylideneaminoato)]osmium(IV) wherein the x and y axes show intrinsic reaction coordinates (IRC) and the z–axis shows energy.

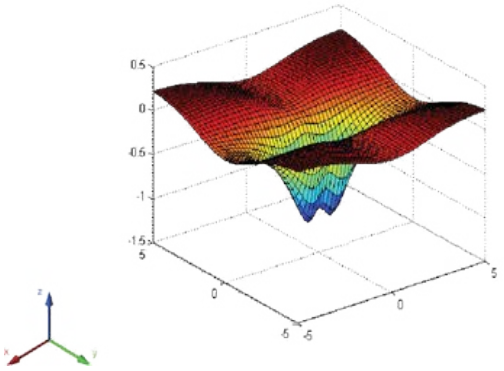

Figure 18 Simulated potential energy surfaces for the formation of Schiff base complex cis-bis(benzenethiolato)[N,N'–ethyl enebis(salicylideneaminoato)]osmium(IV) wherein the x and y axes show intrinsic reaction coordinates (IRC) and the z–axis shows energy.

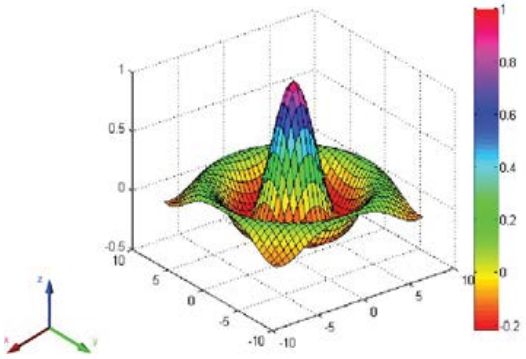

Figure 19 Simulated potential energy surfaces for the formation of Hafnium (IV) Carbide wherein the x and y axes show intrinsic reaction coordinates (IRC) and the z–axis shows energy.

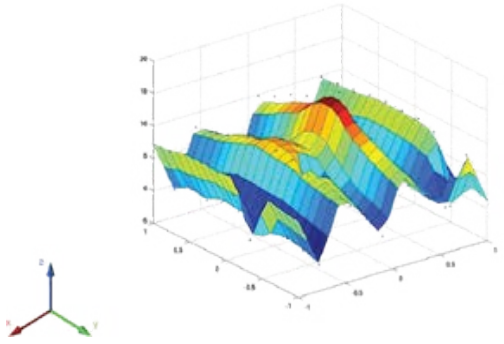

Figure 20 Simulated potential energy surfaces for the formation of Palladium– Hafnium (IV) Carbide wherein the x and y axes show intrinsic reaction coordinates (IRC) and the z–axis shows energy.

ethylenebis(salicylideneaminoato)]osmium(IV) and cis–bis(benzenethiolato)[N,N'–ethylenebis(salicylideneaminoato)] osmium(IV) complexes as the new principal materials at 475°C for 4 hours, nanocomposites of Os-Pd/HfC were successfully synthesized. The results obtained from ATR–FTIR and XRD confirm the purity of compounds due to absence of other peaks. The morphology of the synthesized nanocomposites was evaluated by SEM, TEM and EDX. Shape and size of the synthesized complexes and also the resulted nanocomposites are approximately uniform and identical and their sizes are in the range of 50 and 200 nanometers. The results show that difference on the elementary pre–substance (coordinated amine on the Osmium Schiff base complex) has not a considerable effect on the necessary temperature for producing nanocomposites and their sizes.

Regarding various examined parameters, the best result is obtained from solution containing suspension of the produced Hafnium (IV) Carbides by combustion synthesis at 90°C and pH = 4.9. Using Scherrer equation, grain size of Osmium was calculated as 69 nanometers. Using micro–hardness evaluation test, the hardness of precipitation was measured as 275 Vickers which confirms the structural uniformity of nano. Moreover, using ATR–FTIR, XRD, SEM, TEM and EDX, another proof was achieved for producing this composite and finally, it can be pointed out that it is possible to produce a nanocomposite by a simple method.

Os-Pd/HfC nanocomposites powder was successfully produced by thermochemical method with uniform distribution of Palladium–Hafnium(IV) Carbide particles in the matrix of Osmium. The optimum temperature for creating Palladium–Hafnium (IV) Carbide phase in the obtained nanocomposites was 860°C. In temperatures higher than 850°C, Osmium(IV) Phosphoraniminato and Osmium(VI) Nitrido phases are being created which negatively affect electrical properties of nanocomposites of Osmium matrix. According to the results, complete reduction of Osmium(IV) Phosphoraniminato and Osmium(VI) Nitrido to Osmium are not possible at temperatures higher than 830°C. In the final nanocomposites powder, the size of Palladium-Hafnium(IV) Carbide particles was about 30-60 nanometers.

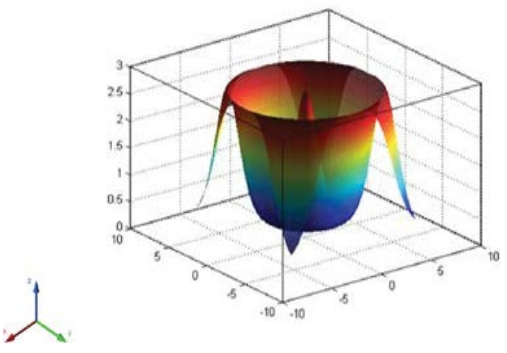

Figure 21 General outline of energy level graph of Os- Pd/HfC nanocomposites wherein the x and y axes show Os–Pd and Os- Pd/HfC bonds' length respectively and also the z–axis shows energy.

References

1 Che C, Cheng WK, Thomas CWM (1986) High-valent Schiff-base complexes of osmium. X-ray crystal structure of trans-bis (benzenethiolato)[N,N'-ethylenebis(salicylideneaminoato)] osmium(IV), Inorganic Chemistry 25: 703-706.

2 Jun-Fang G, Wai-Fun Y, Pui-Ha L, Xiu-Teng W, Song G, et al. (2010) trans[OsIII(salen)(CN)2]−: A New Paramagnetic Building Block for the Construction of Molecule-Based Magnetic Materials, Inorganic Chemistry 49: 1607-1614.

3 Cheung WM, Zhang QF, Ian D, Williams, Wa-Hung L (2007) Synthesis Crystal Structures, and Reactivity of Osmium(II) and -(IV) Complexes Containing a Dithioimidodiphosphinate Ligand, Inorganic Chemistry 46: 5754-5762.

4 Zhang J, Lin LJ, Ru SX, Bing ZH, Yong ZN, et al. (2005) Chiral Osmium Complexes with Sterically Bulky Schiff-Base Ligands. Crystal Structures of Os (IV) Derivatives and the Reactivity and Catalytic Cyclopropanation of Alkenes with EDA, Inorganic Chemistry 44: 3942-3954.

5 Ghosh AK, Kamar KK, Paul P, Peng SM, Lee GH (2002) Photoinduced and Chemical Oxidation of Coordinated Imine to Amide in Isomeric Osmium(II) Complexes of N-Arylpyridine-2-carboxaldimines. Synthesis, Characterization, Electron Transfer Properties, and Structural Studies, Inorganic Chemistry 41: 6343-6350.

6 Wong TW, Lau TC, Wong WT (1999) Osmium (VI) Nitrido and Osmium (IV) Phosphoraniminato Complexes Containing Schiff Base Ligands, Inorganic Chemistry 38: 6181-6186.

7 Li C, Masood KA, George RAB (1998) Nitrosylation of Octaethylporphyrin Osmium Complexes with Alkyl Nitrites and Thionitrites: Molecular Structures of Three Osmium Porphyrin Derivatives, Inorganic Chemistry 37: 533-540.

8 Geun-Bae Y, Li C, Masood A, Khan, George B, et al. (1997) Activation of Thionitrites and Isoamyl Nitrite by Group 8 Metalloporphyrins and the Subsequent Generation of Nitrosyl Thiolates and Alkoxides of Ruthenium and Osmium Porphyrins, Inorganic Chemistry 36: 3876-3885.

9 Ghosh P, Bag N, Chakravorty A (1996) Decarbonylative Metalation of Diformylphenol Schiff Bases: New Osmium and Ruthenium Organometallics Incorporating the Iminium-Phenolato Zwitterionic Motif, Organometallics 15: 3042-3047.

10 Joshua MT, Chu D, Rongzhong J, Gregg DA, Lukehart CM (2003) Synthesis and Characterization of Os and Pt−Os/Carbon Nanocomposites and their Relative Performance as Methanol Electrooxidation Catalysts, Chemistry of Materials 15: 1119-1124.

11 Brian BB, Erik S, Scott L, Werner K, Samuel A (2003) Osmium Phosphiniminato Complexes: Synthesis, Protonation, Structure, and Redox-Coupled Hydrolytic Scission of N−P Bonds, Inorganic Chemistry 42: 4127-4134.

12 Leung CF, Wong TW, Lau TC, Wong WT (2005) Addition of Carbenes to an Osmium(VI) Nitride Complex. Eur J Inorg Chem pp: 773-778.

13 Dehestani H, Kaminsky W, James MM (2003) Tuning the Properties of the Osmium Nitrido Group in TpOs (N) X2 by Changing the Ancillary Ligand, Inorganic Chemistry 42: 605-611.

14 Chiu SM, Wong TW, Man WL, Wong WT, Peng SM, et al. (2001) Facile Nucleophilic Addition to Salophen Coordinated to Nitridoosmium (VI), Journal of the American Chemical Society 123: 12720-12721.

15 Man WL, Chen G, Yiu SM, Shek L, Wong WY, et al. (2010) Formation of μ-dinitrogen (salen)osmium complexes via ligand-induced N-N coupling of (salen)osmium (VI) nitrides, Dalton Trans 39: 11163-11170.

16 Das A, Mobin SM, Lahiri GK (2015) Recognition of fractional non-innocent feature of osmium coordinated 2,2′-biimidazole or 2,2′-bis(4,5-dimethylimidazole) and their interactions with anions, Dalton Trans 44: 13204-13219.

17 Nie HJ, Shao JY, Yao CJ, Zhong YW (2014) Organic–inorganic mixed-valence systems with strongly-coupled triarylamine and cyclometalated osmium, Chem Commun 50: 10082-10085.

18 Das A, Mondal P, Dasgupta M, Kishore N, Lahiri GK (2016) Substituent directed selectivity in anion recognition by a new class of simple osmium-pyrazole derived receptors, Dalton Trans, Advance Article.

19 Beden N, Jirimali HD, Shin W, Ludwig R, Clemens K, et al. (2015) Bio electrochemical Behavior of the Composite PVP-Os/chitosan as a Mediator with Different Types of Enzymes at Graphite Electrode, Insights in Analytical Electrochemistry 1: 8.

20 Heidari A, Brown C (2015) Study of Surface Morphological, Phytochemical and Structural Characteristics of Rhodium (III) Oxide (Rh_2O_3) Nanoparticles. Int J Pharmacology, Phytochemistry and Ethnomedicine 1: 15-19.

21 Chen M, Pan Y, Hoi-Ki K, Zeng JR, Kai-Chung L, et al. (2015) Catalytic oxidation of alkanes by a (salen) osmium (VI) nitrido complex using H_2O_2 as the terminal oxidant. Chem Commun 51: 13686-13689.

22 Esteruelas AM, Fernández I, Gallego MG, Ortíz MM, Molina P, et al. (2013) Mono- and dinuclear osmium N,N′-di- and tetraphenylbipyridyls and extended bipyridyls. Synthesis, structure and electrochemistry. Dalton Trans 42: 3597-3608.

23 Chen G, Wai-Lun M, Shek-Man Y, Wong WT, Szeto L, et al. (2011) Binuclear (salen) osmium phosphinidine and phosphiniminato complexes. Dalton Trans 40: 1938-1944.

24 Albertin G, Antoniutti S, Forcolin M, Gasparato D (2016) Preparation of half-sandwich diazoalkane complexes of osmium. Polyhedron 104: 46-51.

25 Funari V, Meisel T, Braga R (2016) The potential impact of municipal solid waste incinerators ashes on the anthropogenic osmium budget. The Total Env 541: 1549-1555.

26 Yuan Y, Shin H, Kang C, Kim S (2016) Wiring microbial biofilms to the electrode by osmium redox polymer for the performance enhancement of microbial fuel cells. Bio electrochemistry 108: 8-12.

27 Scheller LE, Troiano N, VanHoutan JN, Bouxsein MA, Fretz AJ, et al. (2014) Horowitz, Chapter Seven-Use of Osmium Tetroxide Staining with Microcomputerized Tomography to Visualize and Quantify Bone Marrow Adipose Tissue In Vivo, In: Ormond Macdougald A. Methods in Enzymology 537: 123-139.

28 Pagé P, Sarah-Jane B (2016) The influence of chromite on osmium, iridium, ruthenium and rhodium distribution during early magmatic processes. Chem Geology 420: 51-68.

29 Badanina YI, Malitch NK, Lord AR, Belousova AE, Meisel CT (2016) Closed-system behaviour of the Re-Os isotope system recorded in primary and secondary platinum-group mineral assemblages: Evidence from a mantle chromitite at Harold's Grave. Ore Geology Rev 75: 174-185.

30 Heidari A, Brown C (2015) Study of Composition and Morphology of Cadmium Oxide (CdO) Nanoparticles for Eliminating Cancer Cells. J Nanomed Res 2: 5.

31 Ehrenbrink BP, Waters AC, Kurz DM, Hoffman FP (2016) No evidence of extraterrestrial noble metal and helium anomalies at Marinoan glacial termination, Earth and Planetary Science Letters 437: 76-88.

32 Karmakar S, Mardanya S, Maity D, Baitalik S (2016) Polypyridyl-imidazole based Os(II) complex as optical chemosensor for anions and cations and multi-readout molecular logic gates and memory device: Experimental and DFT/TDDFT study. Sensors and Actuators B: Chemical 226: 388-402.

33 Chor BY, Ganguly R, Leong WK (2016) Convenient route to an electron-deficient Tetraosmium(I) Carboxylate chain. Journal of Organometallic Chemistry 804: 114-117.

34 Jagodish C, Sarker Kh, Uddin MMd, Rahman S, Ghosh S, et al. (2014) Bimetallic osmium-tin complexes: Stannylene and hydrostannylene clusters upon addition of Ph3SnH to unsaturated triosmium clusters [(μ-H)2Os3(CO)8(μ-diphosphine)] (diphosphine = dppm, dppf). Inorganica Chimica Acta 409: 320-329.

35 Liu J, Riches JVA, Pearson DG, Luo Y, Kienlen B, et al. (2016) Age and evolution of the deep continental root beneath the central Rae craton, northern Canada. Precambrian Research 272: 168-184.

36 Suzudo T, Yamaguchi M, Hasegawa A (2015) Migration of rhenium and osmium interstitials in tungsten. J of Nuclear Materials 467: 418-423.

37 Dickson JA, Cohen SA, Coe LA, Davies M, Shcherbinina AE, et al. (2015) Evidence for weathering and volcanism during the PETM from Arctic Ocean and Peri-Tethys osmium isotope records. Palaeogeography, Palaeoclimatology, Palaeoecology 438: 300-307.

38 Chelucci G, Baldino S, Baratta W (2015) Ruthenium and osmium complexes containing 2-(aminomethyl) pyridine (Ampy)-based ligands in catalysis. Coordination Chemistry Reviews 300: 29-85.

39 Gogot J, Poirier A, Boullemant A (2015) Osmium isotopic tracing of atmospheric emissions from an aluminum smelter. Comptes Rendus Geoscience 347: 277-283.

40 Wang F, Zhang T, Zhang Z, Zhang L (2015) Simultaneous separation of noble metals osmium and iridium in simulated leaching of spent catalysts using nano-alumina microcolumn. Separation and Purification Technology 152: 108-114.

41 Ping OS, Ying-Zhou L, Leong WK (2015) Os3(CO)11(BiPh3): The missing link in osmium–bismuth cluster chemistry. J of Organometallic Chem 783: 46-48.

42 Nomaki H, Toyofuku T, Tsuchiya M, Matsuzaki T, Uematsu K, et al. (2015) Three-dimensional observation of foraminiferal cytoplasmic morphology and internal structures using uranium–osmium staining and micro-X-ray computed tomography. Marine Micropaleontology 121: 32-40.

43 Li SL, Ma CY, Zhang QY, Liu XP, Zhang C, et al. (2015) Preparation and characterization of osmium films on quartz substrate by magnetron sputtering method. Surface and Coatings Technology 282: 1-5.

44 Ali Z, Sattar A, Jalali S, Asadabadi, Ahmad I(2015) Theoretical studies of the osmium based perovskites AOsO3 (A=Ca, Sr and Ba). J of Physics and Chemistry of Solids 86: 114-121.

45 Osadebe I, Conghaile PO, Kavanagh P, Leech D (2015) Glucose oxidation by osmium redox polymer mediated enzyme electrodes operating at low potential and in oxygen, for application to enzymatic fuel cells. Electrochimica Acta 182: 320-326.

46 Gannoun A, Vlastélic I, Schiano P (2015) Escape of unradiogenic osmium during sub-aerial lava degassing: Evidence from fumarolic deposits, Piton de la Fournaise, Réunion Island. Geochimica et Cosmochimica Acta 166: 312-326.

47 Vinogradov M, Shul'pina SL, Kozlov NY, Kudinov RA, Ikonnikov SN, et al. (2015) Oxidation of hydrocarbons and alcohols with peroxides catalyzed by new π-cymene osmium complexes. J of Organometallic Chem 784: 52-61.

48 Devanny JA, Baryiames PC, Laperle MC (2015) FTIR investigation of the equilibrium structure of osmium pentacarbonyl in alcohol solvents. Chemical Physics Letters 634: 198-202.

49 Dubin A, Ehrenbrink BP (2015) The importance of organic-rich shales to the geochemical cycles of rhenium and osmium. Chemical Geology 403: 111-120.

50 Chowdhury HA, Rajbangshi S, Rahaman A, Yang L, Nesterov NV, et al. (2015) Phenazine-substituted polynuclear osmium clusters: Synthesis and DFT evaluation of the C-metalated derivatives Os3(CO)9(μ3,η2-C12H7N2)(μ-H) and Os3(CO)9(μ3,η2-C12H6N2)(μ-H)2. J Organometallic Chem 779: 21-29.

51 Yasuhara H, Koga K, Nakashima S (2015) Synthesis and oxidation study of the simplest binuclear metallocene compound of osmium, biosmocene, J of Organometallic Chem 86-90.

52 Liu J, Sharp M, Ash RD, Kring AD, Walker JR (2015) Diverse impactors in Apollo 15 and 16 impact melt rocks: Evidence from osmium isotopes and highly siderophile elements, Geochimica et Cosmochimica Acta 122-153.

53 Chen X, Si C, Gao Y, Frenzel J, Sun J, et al. (2015) Multi-component nanoporous platinum–ruthenium–copper–osmium–iridium alloy with enhanced electrocatalytic activity towards methanol oxidation and oxygen reduction, Journal of Power Sources 324-332.

54 Bezard R, Schaefer FB, Turner S, Davidson PJ, Selby D (2015) Lower crustal assimilation in oceanic arcs: Insights from an osmium isotopic study of the Lesser Antilles, Geochimica et Cosmochimica Acta 330-344.

55 Minami T, Sato T, Minamiki T, Fukuda K, Kumaki D, et al. (2015) A novel OFET-based biosensor for the selective and sensitive detection of lactate levels, Biosensors and Bioelectronics 45-48.

56 Kumar R, Leech D (2015) A glucose anode for enzymatic fuel cells optimized for current production under physiological conditions using a design of experiment approach. Bio electrochemistry 41-46.

57 Mathur P, Raghuvanshi A, Mobin SM (2015) Reactivity of 1,2,3-triselena[3]ferrocenophane towards transition metal carbonyls, Journal of Organometallic Chem 266-273.

58 Schneider JP, Pedersen L, Mühlfeld C, Ochs M (2015) Staining histological lung sections with Sudan Black B or Sudan III for automated identification of alveolar epithelial type II cells, Acta Histochemica pp: 675-680.

59 Sun Y, Ren M, Xia X, Li C, Sun W (2015) Determination of Os by isotope dilution-inductively coupled plasma-mass spectrometry with the combination of laser ablation to introduce chemically separated geological samples, Spectrochimica Acta Part B: Atomic Spectroscopy 22-29.

60 Goto TK, Shimoda G, Anbar DA, Gordon WG, Harigane Y, et al. Molybdenum isotopes in hydrothermal manganese crust from the Ryukyu arc system: Implications for the source of molybdenum. Marine Geology 91-99.

61 Dobson A, Moore DS, Robinson DS, Hursthouse BM, New L (1985) Coordination, oligomerisation and transfer hydrogenation of acetylenes by some ruthenium and osmium carboxylates: Crystal and

molecular structures of bis(trifluoroacetato)carbonyl-(methanol) bis(triphenylphosphine)ruthenium(II) and (1,4-diphenylbut-1-en-3-yn-2-yl)trifluoroacetato-(carbonyl) bis(triphenylphosphine) ruthenium(II), Polyhedron 1119-1130.

62 Bruce IM, Horn E, Shawkataly OB, Snow RM, Tiekink RTE, et al. (1986) Cluster chemistry: LI. Reactions of some substituted ruthenium and osmium cluster carbonyls with dihydrogen. X-ray crystal structures of Ru3(μ-H)2(μ3-PPh)(CO)8(PMePh2), Ru4(μ-H)4(μ-dppm)(CO)10, Ru4(μ- H)3(μ3-PPhCH2PPh2)(CO)10 and Os3(μ-H)2(μ-dppm)(CO)8, J of Organometallic Chem 187-211.

63 Wilczewski T (1986) Cyclopentadienyl-ruthenium and -osmium complexes: VI. Formation and properties of dihydrido-(η-cyclopentadienyl) bis(triphenylphosphine)osmium(IV) cation. Reaction of hydrido(η-cyclopentadienyl)bis(triphenylphosphine)osmium(II) and dihydrido (η cyclopentadienyl)bis(triphenylphosphine)osmium(IV) halogenates with HX acids, X2 dihalogeno and halogenated hydrocarbons, J of Organometallic 307-325.

64 Daifuku H, Yoshimura I, Hirata I, Aoki K, Tokuda K, et al. (1986) Analysis of current-potential curves for mediated electron-transfer reactions at rotating disk electrodes: Electrocatalysis by polypyridine osmium and ruthenium complexes confined to tin oxide electrodes as a Langmuir-Blodgett monomolecular layer, J of Electroanalytical Chem and Interfacial Electrochemistry 47-68.

65 Bruce IM, Cifuentes PM, Humphrey GM, Poczman E, Snow RM (1988) Cyclopentadienyl-ruthenium and -osmium chemistry: XXIX. The effect of chelation on Ru-C(sp2) bond lengths: X-ray structures of Ru(C6H4PPh2)(PPh3)(η-C5H5)-·0.5CH2Cl2 and -(η-C5H5), Journal of Organometallic Chemistry 237-248.

66 Bruce IM, Catlow A, Cifuentes PM, Snow RM, Tiekink RTE (1990) Cyclopentadienyl-ruthenium and -osmium chemistry Part XXXIV. Reactions of 1-alkynes with σ-vinyl-ruthenium complexes. X-ray structures of Ruη3--C5H5) and Ru(η-C5H5)η5-C3(CO2Me)3CHCtBuCH(CO2Me), Journal of Organometallic Chem 187-202.

67 Bruce IM, Koutsantonis AG, Tiekink RTE, Nicholson KB (1991) Cyclopentadienyl-ruthenim and -osmium chemistry: XXXVII. Oligomerisation of C2(CO2Me)2 at a cyclopentadienyl-ruthenium centre: X-ray structures of RuI{η4--(η-C5H5), Ru(η5-C5H5{η5-C6H(CO2Me)6} and Ru(η5-C5H5){η5-Organometallic Chem 271-288.

68 Bruce IM, Koutsantonis AG, Liddell JM, Tiekink RTE (1991) Cyclopentadienyl-ruthenium and -osmium chemistry: XXXVI. Oligomerisation of phenylacetylide residues on ruthenium. Crystal structures of {Ru(PPh3)(η-C5H5)}2(μ-C8Ph4) and {Ru(PPh3)(η-C5H5)}2{μ-C10Ph4(C6H4)}, J of Organometallic Chem 253-269.

69 Amoroso JA, Edwards JA, Johnson FGB, Lewis J, Al-Mandhary MR, et al. (1993) Synthesis of bridged and linked ruthenium and osmium carbonyl clusters containing a [Au2(Ph2PCH2CH2PPh2)]2+ unit. The crystal and molecular structures of Ru5C(CO)14Au2(Ph2PCH2CH2PPh2) and {Os4H3(CO)12}2Au2(Ph2PCH2CH2PPh2), J of Organometallic Chem C11-C13.

70 Sánchez-Delgado RA, Medina M, López-Linares F, Fuentes A (1997) The chemistry and catalytic properties of ruthenium and osmium compounds. Part 7 Regioselective hydrogenation of cinnamaldehyde (3-phenyl-2-propenal) catalyzed by Ru and Os triphenylphosphine complexes in homogeneous solution and by meta-sulfonatophenyl-diphenyldiphosphine (TPPMS) and tris-meta-sulfonato-phenylphosphine (TPPTS) derivatives in an aqueous biphasic system. J of Molecular Catalysis A: Chemical 116: 167-177.

71 Kirbach UW, Folden CM III, Ginter GN, Gregorich KE, Lee DM, et al. (2002) The Cryo-Thermochromatographic Separator (CTS): A new rapid separation and α-detection system for on-line chemical studies of highly volatile osmium and hassium (Z=108) tetroxides, Nuclear Instruments and Methods in Physics Research Section A: Accelerators, Spectrometers, Detectors and Associated Equipment 484: 587-594.

72 Hüffer S, Wieser M, Polborn K, Beck W (1994) Kohlenwasserstoffverbrückte komplexe: XXIX1. Nucleophile addition von carbonylmetallaten an kationische allyl- und alken-komplexe von wolfram, mangan, rhenium, eisen, ruthenium, osmium, cobalt und iridium: zwei-, drei- und vierkernige komplexe mit (σ, π-allyl- und σ-σ-alken-brücken. Journal of Organometallic Chemistry 481: 45-55.

73 Maddock SM, Rickard CEF, Roper WR, Wright LJ (1996) Seven-coordinate dioxygen complexes from dioxygen addition to five-coordinate σ-phenyl, isocyanide-containing derivatives of ruthenium(II) and osmium(II). Crystal structures of OS (η2-O2) (η2-CPh = Np-chlorophenyl) Cl (PPh3)2 and Os (η2-SO4) (η2-CPh = Np-chlorophenyl) Cl (PPh3)2. Journal of Organometallic Chemistry 510: 267-279.

74 Arce AJ, Karam A, Ysaura De Sanctis, Machado R, Capparelli MV, et al. (1997) Ring opening and extrusion of tellurium atoms in the reaction of benzo[b]tellurophene with trinuclear iron, ruthenium and osmium clusters: X-ray crystal structures of [Os2(μ-C8H6Te)(CO)10], [Os4(μ-C8H4)(μ3-Te)(CO11], [Ru(μ-C8H6Te)(CO)6)], [Ru4(μ3-Te)(μ-C8H6)(CO)11] and [Fe2)μ-C8H6Te(CO)6]. Inorganica Chimica Acta 254: 119-130.

75 Younus M, Long NJ, Raithby PR, Lewis J, Page NA, et al. (1999) Synthesis and characterization of mono-acetylide and unsymmetrical bis-acetylide complexes of ruthenium and osmium: X-ray –C6H4-p-–C6H3-o-CH3-p-NO2)] –C6H4-p-–C6H4-p-NO2)]. Journal of Organometallic Chemistry 578: 198-209.

76 Yeuk-Wah HS, Wing-Tak W (1999) Synthesis, characterization and crystal structures of osmium–rhodium mixed-metal clusters containing pentamethylcyclopentadienyl ligand: [Os3Rh(μ-CO)2(CO)9(η5-Cp*)], [Os3Rh2(μ-H)(μ-CO)2(CO)8(η5-Cp) (μ2-η5,η1-CH2C5Me4)] and [Os3Rh(μ3-H)(μ-Cl)(μ-CO)(CO)9(η5-Cp*)]. Journal of Organometallic Chemistry 580: 48-55.

77 Eller S, Trettenbrein B, Oberhuber D, Strabler C, Gutmann R, et al. (2012) Oxidative quenching within photosensitizer–acceptor dyads based on bis (bidentate) phosphine-connected osmium(II) bipyridyl light absorbers and reactive metal sites. Inorganic Chemistry Communications 23: 41-45.

78 Powell CE, Cifuentes MP, McDonagh AM, Hurst SK, Lucas NT, et al. (2003) Organometallic complexes for nonlinear optics.: Part 27. Syntheses and optical properties of some iron, ruthenium and osmium alkynyl complexes. Inorganica Chimica Acta 352: 9-18.

79 Jasimuddin SK, Mostafa G, Sinha C (2004) Mixed ligand complexes of osmium (II)-2,2'-bipyridine: synthesis, spectral characterization and electrochemical properties of bis-chelated-arylazoimidazole-bipyridine-osmium(II) and X-ray crystal structure of [(2,2'-bipyridine)-bis-{1-methyl-2-(p-tolylazo)imidazole}osmium(II) hexafluorophosphate. Inorganica Chimica Acta 357: 1975-1984.

80 Machado RA, Rivillo D, Arce AJ, Sanctis YD, Deeming AJ, et al. (2005) Dinuclear and trinuclear osmium complexes incorporating 1,2-bis(2-pyridyl)ethene as doubly and triply bridging ligands: crystal structures of [Os2(μ:η4-C12H10N2)(CO)6], [Os3(μ-H)2(μ3:η3-C12H10N2)(CO)8] and [Os3(μ-H)(μ3:η4-C12H9N2)(CO)8]. Journal of Organometallic Chemistry 690: 504-512.

81 Amoroso AJ, Johnson BFG, Lewis J, Chi-Keung Li, Carmen Ramirez de Arellano M, et al. (2006) Synthesis and characterisation of the

carboxylate linked osmium clusters [{Os3H(CO)10}2(CO2CH2CO2)], [{Os3H(CO)10}2(CO2C2H4CO2)], [{Os3H(CO)10}2(C4O4)] and [{Os3H(CO)10}2(C4O4){Co2(CO)6}]. Inorganica Chimica Acta 359: 3589-3595.

82 Peña D, Otero Y, Arce A, Díaz L, Ysaura De Sanctis, et al. (2014) Synthesis and characterization of trinuclear osmium clusters containing diallylphosphines as hemilabile ligands: Experimental and theoretical studies of their reactivity with nucleophilic molecules. Journal of Organometallic Chemistry pp: 772-773.

83 Wrobel K, Figueroa JAL, Zaina S, Lund G, Wrobel K (2010) Phosphorus and osmium as elemental tags for the determination of global DNA methylation-A novel application of high performance liquid chromatography inductively coupled plasma mass spectrometry in epigenetic studies. Journal of Chromatography B 878: 609-614.

84 Hunt SW, Yang L, Wang X, Richmond MG (2011) New osmium cluster compounds containing the heterocyclic ligand 2,3-bis-(diphenylphosphino)quinoxaline (dppq): Ligand isomerization and crystal structures of dppq, the isomeric clusters Os3(CO)10(dppq), and HOs3(CO)9[μ-2,3-PhP(η1-C6H4)(Ph2P) quinoxaline]. Journal of Organometallic Chemistry 696: 1432-1440.

85 Young KJH, Lokare KS, Leung CH, Mu-Jeng Cheng, Nielsen RJ, et al. (2011) Synthesis of osmium and ruthenium complexes bearing dimethyl (S,S)-2,2'-(pyridine-2,6-diyl)-bis-(4,5-dihydrooxazol-4-carboxylate) ligand and application to catalytic H/D exchange. Journal of Molecular Catalysis A: Chemical 339: 17-23.

86 Burton AW, Ong K, Rea T, Chan IY (2009) On the estimation of average crystallite size of zeolites from the Scherrer equation: A critical evaluation of its application to zeolites with one-dimensional pore systems. Microporous and Mesoporous Materials 117: 75-90.

87 Alfred D'Agostino T (1992) Determination of thin metal film thickness by x-ray diffractometry using the Scherrer equation, atomic absorption analysis and transmission/reflection visible spectroscopy. Analytica Chimica Acta 262: 269-275.